LAGRANGE: LAser GRavitational-wave ANtenna at GEo-lunar L3, L4, L5

John W. Conklin [1], Sasha Buchman, Karthik Balakrishnan, Robert L. Byer, Grant Dufresne Cutler, Dan B. DeBra, Eric Hultgren, Brian Lantz, John A. Lipa, Shailendhar Saraf, Andreas Zoellner
W.W. Hansen Experimental Physics Laboratory, Stanford University, Stanford, CA 94305-4085 [7]

Dohy M. Faied, Cyrus Foster, Anthony L. Genova, Belgacem Jaroux, Hugo S. Sanchez, Simon. P. Worden
NASA Ames Research Center, Moffett Field, CA 94035 [5]

Ahmad Aljadaan, Abdul Alfauwaz, Mohammad Almajed, Haithem Altwaijry, Turki Al-Saud
King Abdulaziz City for Science and Technology, Riyadh, Saudi Arabia 11442 [3]

John Hanson
CrossTrac Engineering, Inc. Sunnyvale, CA [2]

Dan Bower, Bill Costello, Ken Hooper, Andy Klavins, Alice Palmer, Barbara Plante, David Schaechter, Tom Sherrill, Eric Smith, Ker-Li Shu, Domenick Tenerelli, Roel Vanbezooijen, Gopal Vasudevan
Lockheed Martin Space Systems Company, Palo Alto, CA 94304 [4]

Victor Aguero, Scott D. Williams
SRI International, Menlo Park, CA 94025-3453 [6]

This white paper describes a space gravitational wave mission concept consisting of three drag-free spacecraft at the Earth-moon L3, L4, and L5 Lagrange points. It also describes a Gravitational Reference Sensor (GRS) instrument concept, an Interferometric Measurement System (IMS) concept, and enabling technologies for drag-free propulsion, charge management and material coatings. The primary submitter is John W. Conklin for the team members listed above. We are willing to present this concept at the workshop and there is no sensitive or controlled information herein.

INTRODUCTION

Stanford University, NASA Ames Research Center, Lockheed Martin, the King Abdulaziz City for Science and Technology (KACST), and SRI International have formed a collaboration (called SALKS in this paper) to develop a new space gravitational-wave observatory mission concept, named LAGRANGE, which maintains all important LISA science at reduced cost and with reduced technical risk. We achieve this goal by revisiting all aspects of LISA for possible improvements, while structuring the new elements to be modular and scalable, as well as interchangeable with baseline LISA systems. We incorporate both new technologies developed after the LISA and LISA pathfinder designs (UV-LEDs, non-transmissive optics, SRI thrusters, TM coatings and others), as well as older space qualified technologies from Honeywell (1953), DISCOS (1972) [49], GP-B (2004) [29].

LAGRANGE comes close to meeting the LISA sensitivity below 10 mHz and exceeds it at higher frequencies (see Fig. 1). An internal NASA cost analysis, cross checked against previous mission data, gives a Rough-Order-of-Magnitude (ROM) cost of $950M, with 30% margin, significantly less than the current LISA cost [31], while including many technical advantages.

The three main elements of a space-based gravitational-wave observatory are 1) the constellation and its orbit 2) the gravitational reference sensors, and 3) the metrology system (see Table I for comparison of LAGRANGE to LISA). The following are the discriminating improvements of LAGRANGE.

TABLE I: Top-level LISA / LAGRANGE comparison.

	LISA	LAGRANGE
Number of spacecraft	3	3
Orbit	heliocentric, 20° Earth trailing	Earth-moon L3, L4, L5
Wet launch mass	~5,000 kg	2,070 kg
Arm length	5 Gm	0.67 Gm
IMS sensitivity	18 pm $\mathrm{Hz}^{-1/2}$	5 pm $\mathrm{Hz}^{-1/2}$
DRS accel. noise	3 fm/s^2 $\mathrm{Hz}^{-1/2}$	3 fm/s^2 $\mathrm{Hz}^{-1/2}$
Observation period	5 yr	5 yr
Telescopes / spacecraft	2 × 40 cm	2 × 20 cm
GRSs / spacecraft	2	1
Optics benches / spacecraft	2	1
Laser power / spacecraft	2 × 1.2 W	1 × 1 W
Beam steering	articulated optics & GRS	in-field pointing

1. LAGRANGE consists of a triangular constellation of identical spacecraft (S/C) and payload at the Earth-moon L3, L4, and L5 Lagrange points. This is the most stable geocentric configuration. Launch of the 3 spacecraft with one small propulsion module is possible on a Falcon 9, which costs $118M (NASA Launch Services). Earth-based receivers are continuously in the field of view of fixed transmitters on each spacecraft increasing the communication bandwidth by >100 from LISA and greatly reducing data latency (hours instead of days). From the experience with GP-B and LIGO, the closest analogs to date, this large bandwidth is an absolute requirement for mission success.

2. The single Gravitational Reference Sensor (GRS) is based on the Modular Gravitational Reference Sensor (MGRS) concept developed by SALKS and consists of a spherical test mass (TM) spinning at 3-10 Hz thus providing frequency separation from the 1 mHz to 1 Hz primary LAGRANGE bandwidth. Similar TMs have been successfully flown on DISCOS, and GP-B. The MGRS is true drag-free with no forcing in any direction, and has a 35 mm gap that can be increased if necessary. Caging by a single screw mechanism was demonstrated on the DISCOS flight and is critical to the risk reduction in LAGRANGE versus LISA. Magnetic spin-up and polhode damping were demonstrated thoroughly in Honeywell gyroscopes.

3. The Interferometric Measurement System (IMS) consists of a single laser and optics bench that incorporates only reflecting elements in the critical locations: gratings and mirrors, while laser frequency stabilization is enhanced by high finesse optical cavities and/or iodine molecular clocks. Two telescopes per S/C with in-field pointing are designed to minimize path-length errors.

Significant cost reduction for LAGRANGE over LISA was principally achieved in two ways: (a) by decreasing the per spacecraft mass and power by reducing payload components (2 lasers, 2 GRSs, and 2 optics benches for LISA was reduced to 1 of each for LAGRANGE), and (b) by using a geocentric orbit, which requires only one propulsion module for all three spacecraft and reduces mission operations complexity by increasing communications bandwidth.

There is incremental risk reduction in LAGRANGE due to an emphasis on simplicity. In addition, the SALKS collaboration is implementing flight demonstrations of critical technologies on small satellites and CubeSats [57]. These include charge management, laser frequency stabilization, shadow and interferometry position measurement, thrusters and caging mechanisms. The charge management flight (UV LED Sat [50]) is scheduled for 2013.

The structure of this paper is as follows: we start with a very brief summary of the science capabilities; follow with the design overview and science orbit; discuss LAGRANGE specific details of the proposed instrument, focusing on the Interferometric Measurement System (IMS) and the Disturbance Reduction System (DRS); describe the mission and spacecraft design, and the cost estimate; closing with a discussion of TRLs.

SCIENCE CAPABILITIES

The primary measurement band for LAGRANGE is 1 mHz to 1 Hz, where the strain sensitivity is 3×10^{-20}. The target astrophysical sources include:

1. Massive black hole mergers in the range of 10^4 (MBH) to 10^7 (SMBH) solar masses with orbit periods of 10^2 to 10^4 sec, giving signal-to-noise (SNR) ratios up to several thousands out to $z \sim 15$.

2. Merging of stellar mass compact objects with massive black holes (EMRI) with signal periods of 10^2 to 10^3 seconds.

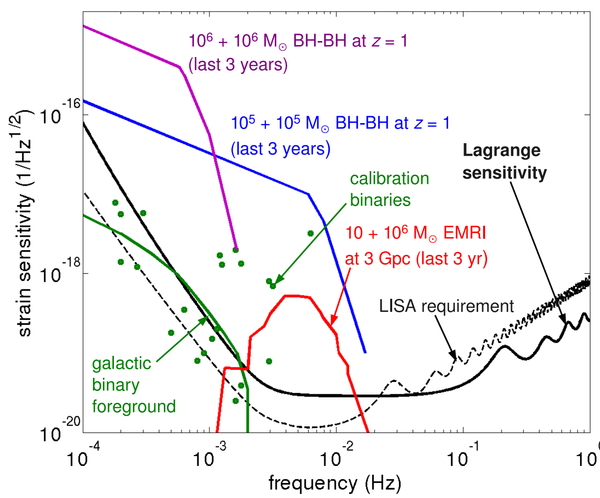

FIG. 1: LAGRANGE strain sensitivity, and comparison with LISA requirements and gravitational wave sources.

3. Stellar mass binaries within the Milky Way with orbital periods of 10^2 to 10^3 seconds.

Figure 1 shows the estimated LAGRANGE strain sensitivity (solid black curve) in units of $\mathrm{Hz}^{-1/2}$, compared to the LISA requirement (dashed curve). Colored curves and points represent the various known sources within the LAGRANGE bandwidth. The green curve is the confusion noise from unresolved galactic binaries that dominates instrumental noise between 5×10^4 and 2×10^3 Hz. All sources above the sensitivity curve are detectable by LAGRANGE. The green points represent the frequencies and strengths of known Galactic binaries; their height above the noise curve gives their SNR. The purple, blue and red curves represent sources (two SMBH binaries, and an EMRI, respectively) whose frequency evolves upward during LAGRANGE's observation.

Sensitivity normal to the ecliptic plane is less than that of LISA due to the reduced out-of-plane motion of the observatory. However, higher gravitational-wave harmonics provide a significant improvement to position determination of MBH binaries [56], and locating spinning black holes in a black hole binary is much more accurate than would be expected from the modulation produced by LISAs precessing plane alone [42, 56].

LAGRANGE will achieve all three of the most important science goals of LISA listed in the 2010 astrophysics decadal survey, "New Worlds, New Horizons" [31]:

1. Measurements of black hole mass and spin will be important for understanding the significance of mergers in the building of galaxies;

2. Detection of signals from stellar-mass compact stellar remnants as they orbit and fall into massive black holes would provide exquisitely precise tests of Einstein's theory of gravity; and

3. Potential for discovery of waves from unanticipated

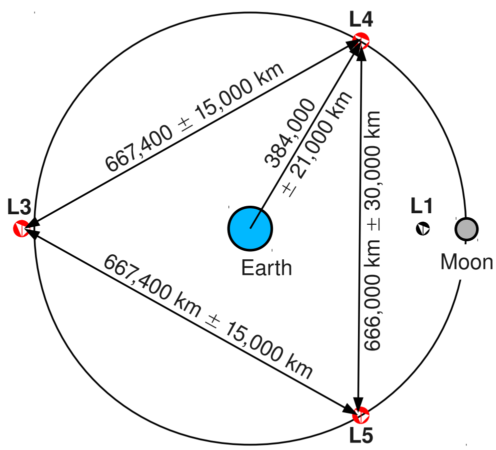

FIG. 2: Orbit design with 3 drag-free spacecraft at the Earth-moon L3, L4, and L5 LAGRANGE points.

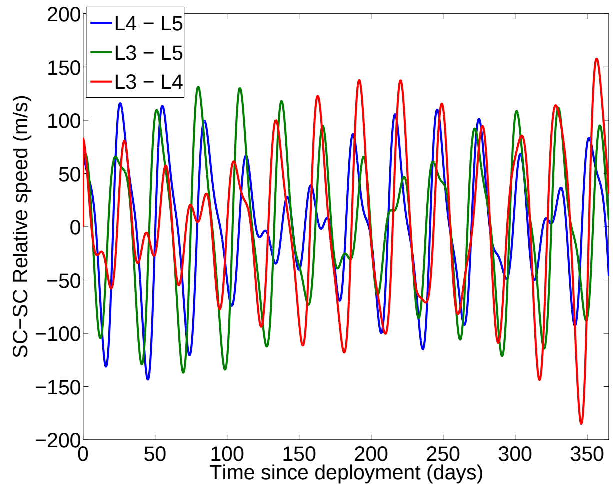

FIG. 3: LAGRANGE S/C-to-S/C range rates over 1 year.

or exotic sources, such as backgrounds produced during the earliest moments of the universe or cusps associated with cosmic strings.

OBSERVATORY DESIGN OVERVIEW

LAGRANGE consists of a triangular constellation of three identical spacecraft at the L3, L4, and L5 Lagrange points of the Earth Moon (E-m) system (see Fig. 2). This is the most stable geocentric configuration and has an average arm length of 670,000 km. Detection and observation of gravitational waves is performed using laser interferometry to measure the distances between inertial references in each spacecraft as in LISA [19]. Each spacecraft contains a single spherical MGRS as the inertial reference and a single optical bench serving as a metrology reference. The light source is a 1 W 1064 nm wavelength laser, while two 20 cm aperture telescopes send and receive laser light to and from the remote spacecraft.

The fundamental measurement scheme is based on the LISA approach. The interferometric science measurement is made in two steps. The first is the short-arm interferometer, which measures the optical bench position with respect to the test mass (TM) center of mass. The second is the long-arm interferometer that measures the distance from the local optical bench to the optical bench on the remote spacecraft. Time Delay Interferometry (TDI) [15] combines phase measurements made on-board each spacecraft, accounting for the light travel time between spacecraft to cancel laser noise while retaining the gravitational wave signal.

SCIENCE ORBIT

While the Earth-moon Lagrange points provide the most stable geocentric orbits, the gravitational attraction of the sun generates some instability. The initial position and velocity of each spacecraft have been chosen to maximize the time between station keeping maneuvers of < 1 m/s once every 6-12 months, performed using the on-board micronewton propulsion system.

TABLE II: Comparison of E-m L3, L4, L5 and LISA orbits.

Parameter	EM L3, L4, L5	LISA
Nominal arm length	670,000 km	5,000,000 km
Max. arm length variation	$\lesssim 5$ %	1%
Breathing angle range	$\pm \lesssim 5$ deg	± 0.5 deg
Max. SC-to-SC range rate	$\lesssim 150$ m/s	10 m/s
Variation of orbit plane	5 deg	60 deg

Table II compares the stability and orbital dynamics of the Earth-moon L3, L4, L5 orbit with that of LISA. Further improvement in the stability of the LAGRANGE constellation is expected through simultaneous optimization of the initial conditions for all three spacecraft, minimizing range rate and breathing angle variations. The spacecraft at L3 follows a perturbed halo orbit, roughly 50,000 km in diameter and canted with respect to the plane of the moon's orbit by $\sim 45°$. The spacecraft at L4 and L5 follow semi-periodic orbits as well, but with more complex geometries. One of the alternatives under study is to place all three spacecraft in periodic orbits with similar phases, thus reducing range rate variations.

The initial orbit design exhibits dynamics 5 to 10 times larger than LISA. Range rates between spacecraft vary by ± 150 m/s, as shown in Fig. 3. This means that if the transmitted laser frequency is held constant, the on-board phase measurements must accomodate heterodyne frequencies of $\lesssim 150$ MHz, compared with < 20 MHz for LISA. However, since the range rates to the two remote spacecraft exhibit large common mode variations (see Fig. 3), tuning the laser frequency on each spacecraft to the mean of the two known Doppler frequencies, reduces the heterodyne frequency to $\lesssim 50$ MHz. The telescope must accomodate $\pm$ 2.5 deg of beam steering for the IMS to remain locked to the remote spacecaft.

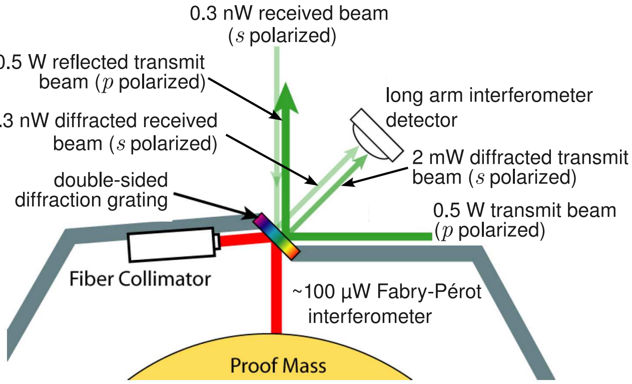

FIG. 4: Primary IMS configuration using a diffraction grating as the reference surface and beam splitter. The readout for the short-arm interferometer is not shown.

INTERFEROMETRIC MEASUREMENT SYSTEM

Interferometry

The IMS has two main components: The short-arm interferometer determines the distance from the optics bench to the mass center of the TM, and the long-arm interferometer measures the distance from the optics bench to the optics bench on the remote spacecraft. The combined TM-to-TM one way measurement accuracy is 8 $\mathrm{pm\,Hz^{-1/2}}$ (4 $\mathrm{pm\,Hz^{-1/2}}$ shot noise limit). While the internal interferometer measures distances that vary by $<\ \lambda$ during science operations, the external interferometer must accommodate Doppler shifts of $\lesssim$ 150 MHz due to spacecraft-to-spacecraft range rates.

Both long and short-arm interferometers are supplied by a single 1 W NPRO laser that is fiber linked to a single optical bench. Once on the bench, all metrology is done with free-space optics. Two 20 cm aperture telescopes per spacecraft send and receive laser light to and from the remote spacecraft. A phasemeter is used to measure the long-arm interferometer phase to 1 μcycle $\mathrm{Hz^{-1/2}}$ in the measurement band.

Optical Bench: Once on the optics bench, a small portion of the 1 W beam is divided off and fed into the frequency stabilization system, shown as the Electro-Optic Modulator (EOM) plus optical cavity in Fig. 5. The main beam then passes through a 50/50 beam splitter, which divides the power between the right and left arms.

Two interferometer configurations have been studied. The primary configuration utilizes a single double-sided diffraction grating to act as the main reference surface and as a beam splitter (see Fig. 4). For both left and right arms, the 1/2 W beam is s polarized so that most of its power reflects off of the polarization selective, high efficiency grating and is sent to the telescope (dark green beam in Fig. 4). A small portion of this beam is diffracted at 45 deg due to the imperfect grating efficiency and strikes a photodetector. The incoming light from the remote spacecraft is p polarized and therefore almost all ($\sim$ 0.3 nW) of it is diffracted off at 45 deg and interferes with the local beam at the detector. The short-arm interferometer is fed from a tap-off from the main laser using fiber, delivering $\sim$ 100 μW of power to the grating. The back side of the grating is Littrow mounted and focusing in order to form a Fabry-Pérot cavity between the TM and the grating (red beam in Fig. 4). A finesse-enhanced Fabry-Pérot cavity allows a two-point measurement between the grating and TM, without the use of a reference arm of a Michelson interferometer. The Pound Drever-Hall (PDH) technique [28] allows the measurement to be made at frequencies where the laser is quantum-noise-limited. A short-arm interferometer using a Littrow mounted grating has been demonstrated in the lab at Stanford [13].

The primary interferometer configuration using a double sided grating has several advantages: (a) It provides a single, well defined reference surface that separates the long and short arm interferometers. (b) It can be made from a thin, low CTE material that reduces thermally induced path-length errors relative to transmissive optics where much higher dn/dT effect are important. (c) It greatly reduces the number of optical components needed and decreases the size of the optics bench.

The back-up configuration is more LISA-like, utilizing a larger bench with bonded optical components (see Fig. 5). A low power portion of the 1/2 W beam for each arm is picked-off and used for both the short-arm interferometer and the long-arm interferometer. The short-arm interferometer is a Michelson interferometer, while the long-arm interferometer simply interferes the local and received beams. A lens or mirror is used to focus the beam at the center of the TM so that most of the light is reflected back to the interferometer.

On the frequency stabilization section of the bench, the low power laser pick-off is fed through an EOM which adds RF tunable sidebands to the laser frequency. One of the sidebands is then locked to a nominal 10 cm optical cavity, with a Free Spectral Range (FSR) of 1.5 GHz. Locking is performed using PDH via $\sim$ 10 MHz sidebands added to the main sidebands. The main rf sidebands are tuned with a maximum range of FSR/2 in order to shift the carrier frequency by the same amount. Sideband locking for frequency tunable stabilized lasers has been considered for LISA and demonstrated in a laboratory envinronment [44]. This technique is optically more efficient than using an Acoust-Optic Modulator (AOM). Initial tuning is performed during the initialization phase of the mission in order to set the laser frequency on each spacecraft to the optimal offset. The offset can then be held constant or tuned continuously to accomodate any changes in the cavities or Doppler rates to maintain optimal detection frequency and receiver performance. Tuning the laser frequency offset to follow the mean Doppler frequency of the two remote spacecraft reduces the heterodyne frequency measured by the phase meter from $\lesssim$ 150 MHz to $\lesssim$ 50 MHz.

Phasemeter: The phasemeter measures the phase of the long-arm interferometer beat note to 1 μcycle $\mathrm{Hz^{-1/2}}$ over

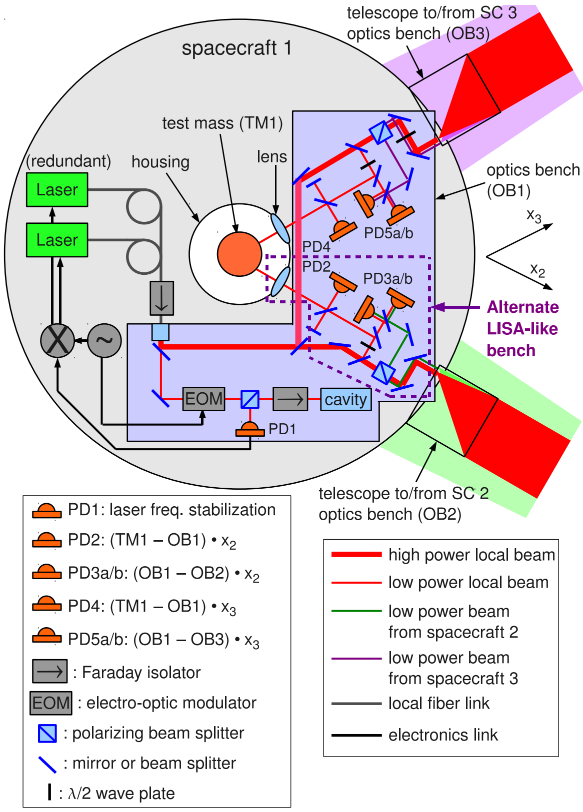

FIG. 5: IMS and MGRS block diagram, with the alternate LISA-like optics bench. The primary grating based design replaces all components inside the dotted lines.

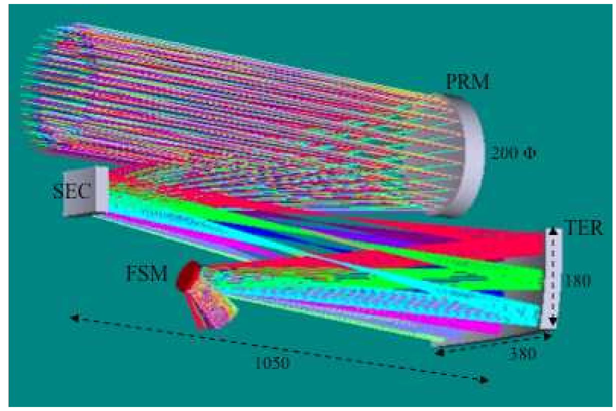

FIG. 6: Stage one of the LAGRANGE telescope.

1 mHz to 1 Hz. The phasemeter uses a high-speed analog to digital conversion followed by a digital phase locked loop, as in the LISA design [48]. The phasemeter has to accommodate a heterodyne frequency of $\lesssim$ 50 MHz, assuming continuously tuned laser frequency offsets. Improvements in the LAGRANGE constellation orbit may reduce this range further.

Point-Ahead Angle Mechanism: A small actuator located on the optics bench (not shown on Fig. 5) angles the output beam with respect to the input beam $\sim 7\ \mu$rad to accommodate the distance that the remote spacecraft has traveled in 2.2 light sec. path length variations must be less than 1 pm and beam jitter less than 20 nrad. The Point-Ahead Angle Mechanism developed for LISA meets LAGRANGE requirements [45].

Telescope

The main design challenges for the LAGRANGE telescope are: a 5 deg field of regard (FOR) to accommodate constellation geometrical changes, minimized entrance aperture size to satisfy radiometric requirements, $\sim$ 1 mm internal beam size for compatibility with the metrology system, and 5 pm pathlength stability.

The FOR and magnification combined dictate a minimally two-stage design, and minimizing stray light, leads to an off-axis un-obscured system that is within the capabilities of recently flown design apertures, geometric tolerances, and wavefront stability. Stage one, shown in Fig. 6, is a 6:1 Three Mirror Anastigmat (TMA) that relays the entrance pupil to a small steering mirror. It has nearly diffraction-limited performance over the FOR, with a scan mirror located near its exit pupil to scan over the Field of View (FOV) (physical motion of a single scan mirror is 15 deg). Such scan mirrors can be designed to ensure no motion of the center of mass (CM) while slewing, and back-to-back design will also ensure no change in CM and gravity gradient. An additional 33$\times$ stage completes the 200$\times$ beam expander. Design of this stage is relatively straightforward, since it has a narrow FOV and the system is monochromatic. The un-obscured TMA is a spaceflight-proven optical design from (QuickBird [30], MTI [38]) and has been used successfully by Lockheed Martin for laser-com applications. It may be possible to simplify the beam steering design by taking advantage of advances in precision laser scanners based on acousto-optic or electro-optic deflectors that can achieve precision beam steering without moving parts [41, 55].

A low CTE composite metering structure, such as an M55J/954-3, combined with mK temperature control achieved using heaters and temperature sensors, can be used to control Optical Path Difference (OPD) changes due to CTE variations to the pm level.

OPD induced by steering through the FOR is ~ 100 pm/μrad averaged over the field. Given a 5 deg/27.3 day (lunar orbital rate) field rate of change, the expected OPD over 1000 seconds is of order 3,600 pm, which is calibrated to 10^{-3} or compensated at the FOR mirror.

The use of the off-axis TMA for space-based imaging has significant heritage, and is considered TRL 9. Although mK temperature control, the use of very low CTE composite telescope structures and pm pathlength monitoring have flight qualification test heritage, the combination of the three to produce a pm-stable system is new technology, and is TRL 4.

Each spacecraft has two identical telescopes. Both are actuated so that the fixed high gain communications antenna remains nominally pointed at the Earth, and to provide redundancy in case of failure.

During brief periods, twice per year, the line-of-sight to the remote spacecraft will come within 5 deg of the sun. Existing flight-qualified narrow band filters are used to block sunlight from entering the telescope and damaging the IMS. A thin, low CTE window (or coating) is placed either at the front end of the telescope, which reduces overall solar heating to the telescope, or at the back end, allowing for a much smaller ($\sim$ 1 cm) filter, or possibly at both locations.

Metrology Error Budget

A detailed error budget for the IMS has been assembled. It contains four main contributions, each with several sub-entries. The four main contributions and associated error at 3 mHz are: shot noise (4 pm $\mathrm{Hz}^{-1/2}$), optical path length errors (5 pm $\mathrm{Hz}^{-1/2}$), residual USO phase noise (3 pm $\mathrm{Hz}^{-1/2}$), and residual laser phase noise (3 pm $\mathrm{Hz}^{-1/2}$). The total error at 3 mHz is 8 pm $\mathrm{Hz}^{-1/2}$. The IMS error is nearly flat at higher frequencies, and exhibits a $1/f^2$ trend below 3 mHz.

The shot noise is limited by the laser output power, arm length and telescope aperture size, while the optical path length error is dominated by the telescope design with its required 5 deg beam steering. Achieving the allocated residual clock noise in the presence of a large Doppler frequency ($\lesssim$ 50 MHz) requires a clock $\sim$ 5 times better than the LISA USO.

DISTURBANCE REDUCTION SYSTEM

Modular Gravitational Reference Sensor

The SALKS collaboration includes leaders in the field of Gravitational Reference Sensor technology that have developed and flown GRSs for the only two spacecraft operated in "true" drag-free mode (without any TM support forces): Triad I [49] and Gravity Probe B [18]. Based on this experience, a spherical geometry was chosen for the LAGRANGE GRS. A spherical GRS for LISA has been proposed as early as 1998 [25, 40], and has advantages that outweigh its disadvantages. They are:

- No TM forcing or torquing: neither electrostatic support nor capacitive sensing is required, reducing disturbances and complexity,
- Large TM-to-housing gap (35 mm): disturbances are reduced and spacecraft requirements are relaxed,
- A long flight heritage [26]: Honeywell gyroscopes, Triad I and GP-B,
- Scalability: performance can be scaled up or down by adjusting TM and gap size,
- Simplicity: no cross coupling of degrees of freedom,
- A simple flight-proven caging mechanism.

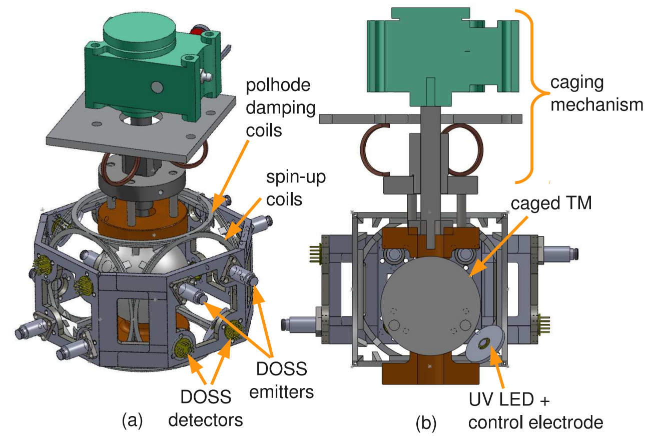

FIG. 7: (a) Modular Gravitational Reference Sensor isometric view, and (b) cross-section with the test mass caged.

This GRS concept, now called the Modular Gravitational Reference Sensor (MGRS) has been under development at Stanford with support from NASA and KACST for a wide range of applications since 2004 [20, 52]. The primary components of the MGRS, shown in Fig. 7, include a spinning spherical TM, a differential optical shadow sensor system for drag-free control, a caging (launch lock) mechanism based on the flight-proven DISCOS design, magnetic coils for test mass spin-up to 3-10 Hz and polhode damping, based on the Honeywell design, and a charge control system based on the GP-B design but using modern LEDs as UV sources.

Note that the LISA Pathfinder GRS [27], the baseline GRS for LISA, is expected to demonstrate 3×10^{-14} m/s $\mathrm{Hz}^{-1/2}$ above 1 mHz during the LISA Pathfinder mission [14]. Assuming a successful flight demonstration, the Pathfinder GRS could be utilized. A single LISA Pathfinder GRS per drag-free spacecraft has been studied [32] and would principally require modifications to the optical bench design.

Spinning Spherical Test Mass: The nominal test mass is a 2.9 kg, 70 mm diameter sphere of 70%/30% Au/Pt. An alternate material is Berglide (2%/97.5%/0.5% Be/Cu/Co), a common, well studied material, easier to fabricate with 10^{-6} magnetic susceptance, but less dense by a factor > 2.

The TM must be round to $\lesssim$ 30 nm, similar in roundness to the GP-B flight rotors [39], and have a mass unbalance $\lesssim$ 300 nm, 30 times larger than that of the GP-B rotors. Internal axi-symmetric sections of the TM are hollowed out to produce a moment of inertia difference ratio of 10%, while reducing the average density by 20% [22]. The resulting polhode frequency is 0.3-10 Hz, at the high end of the LAGRANGE science band. The hollow sections also allow the mass center to be moved within the sphere through an iterative measurement/re-shaping procedure in order to meet the mass unbalance requirement [22]. Laboratory measurement of the mass unbalance of a 50 mm spherical TM has been demonstrated to 200 nm [24]. For a GRS housing vented to space, the pressure is 10^{-6} Pa, resulting in a spin-down time $\sim$ 4,000 years.

Interferometric measurement of the surface of a sphere has also been demonstrated in the lab [13], and spinning of the sphere averages geometric irregularities, allowing for determination of the mass center. A computationally simple and robust on-board algorithm for determining the mass center to pm accuracy has been developed analytically [23] and demonstrated numerically [12]. The TM external geometry requires no special markings or cut-outs, and pm-level knowledge of the sphere's geometry is not needed.

The TM spin axis is normal to the constellation plane ($\pm$ 5 deg) to achieve maximum averaging of geometric irregularities. Systematic measurement errors due to the axisymmetric harmonics of the sphere's geometry remain below 1 pm as long as the out-of-plane spacecraft motion is $< 3\,\mu\mathrm{rad\,Hz^{-1/2}}$ and the maximum rate is $< 0.6\,\mu$rad/s [23]. The former requirement is bounded by the $< 10\,\mathrm{nrad\,Hz^{-1/2}}$ attitude motion requirement for the IMS, and the latter is greater than the maximum attitude rate ($\sim$ $0.2\,\mu$rad/s) needed to maintain pointing throughout the orbit.

The TM is coated in a carbide compound (e.g. SiC or ZrC), which provides a hard, conductive, and highly reflective surface. SiC and ZrC have quantum efficiencies 15-30% of that of gold, thus supporting UV charge control. A major advantage of these coatings over gold is their low adhesion to other surfaces. The coating of the TM and MGRS, which has no sensitive surfaces, are designed such that the TM can repeatedly touch the housing wall in a μg environment without damaging the TM or housing or sticking. This greatly simplifies the caging design and means that during low thrust station keeping maneuvers (once every 6-12 months), the TM need not be re-caged, but only spun down to a low level.

Shadow Sensor for Drag-free Control: The Differential Optical Shadow Sensor (DOSS) requires two pairs of parallel beams for a three dimensional position measurement [59]. A total of 4 pairs is planned for redundancy. Superlumniscent LEDs (SLEDs) with a wavelength of 1550 nm are used for the light source. The target sensitivity is $1\ \mathrm{nm\,Hz^{-1/2}}$ over the drag-free control bandwidth. The low frequency noise floor is improved with lock-in amplification and modulation of the beam power.

Caging: The function of the caging system is to secure the test mass during launch and ascent when the satellite can be expected to experience high static accelerations (up to 6 g [8]), random vibration up to 14.1 g rms [34], and shock up to 3000 g at payload separation [8].

The caging mechanism for the MGRS is based on the flight proven design for DISCOS, which applied a load of 43 g to the TM [33]. The caging system will passively maintain a high compression pre-load until deployment in orbit when the TM will be released with low residual velocity. The TM and housing are designed such that they will contact several times with $\sim$ mm/s velocities, with no damage, until sufficient kinetic energy is absorbed and the drag-free control system is able to capture the TM.

The test mass is clamped between two holding tubes, one of which is driven by a trapezoidal jack screw (see Fig. 7). The surface finish for the holding tubes and the TM will be of dissimilar materials to avoid residual adhesion. The jack screw is self-locking to passively maintain compression force, and is driven by a piezoelectric motor which is also self-locking. BeCu ring springs oppose the compression force of the jack screw, such that at full load, the opposing surfaces that retain the springs will engage a limit switch, and stop the jack screw.

Spin-up Mechanism: The spin-up of the TM is performed with a rotating magnetic field similar to the ones used in Honeywell gyroscopes [43]. Four magnetic coils separated by 90 deg in the constellation plane are excited with ac currents to create the rotating magnetic field and will perform spin-up within a few hours. Two additional magnetic coils aligned normal to the constellation plane create a dc field for polhode damping and spin-axis alignment (see Fig. 7). The TM can also be spun-down by reversing the phase of the ac currents.

Charge Control: Charge management by UV photoemission using the 254 nm line of an rf mercury source was succesfully demonstrated by the GP-B mission in 2004-2005. Newer technology allows the use of commercially available LEDs available in the 240-255 nm range [51] as the UV source. These devices are fast switchable (f $>$ 100 MHz), allowing pulse timing to be synchronized to a control electrode. With a 10 mA driving current, these LEDs are capable of generating 10 μW at 252 nm [17]. Electrons are generated through photoemission from the TM and control electrode. The direction of charge transfer is selected by setting the phase between the UV-LED and control electrode [51]. Measurement of the TM potential can be performed in several ways, including the force modulation used in GP-B and contactless dc measurement of the electric field. Passive charge management, relying on a virtual "wire" generated by photoemission and without bias is also practical for the proposed low ($\sim$ 5 pF) capacitance MGRS. The power and mass per GRS are estimated at 2-3 W and 200-300 g, respectively. A number of UV-LED models have successfully completed environmental testing [17, 53].

Micronewton Thrusters

Drag-free translational control and spacecraft pointing are both actuated by a micronewton electric propulsion system. The requirements for precision and noise are equivalent to those for LISA: 0.1 $\mu\mathrm{N\,Hz^{-1/2}}$ thrust noise from 1 mHz to 1 Hz and 0.1 μN thrust precision. Busek Colloid Micro-Newton Thrusters (CMNT) meet both of these requirements. Further development is required to meet the 5 year lifetime goal [36, 58].

In addition to the Busek CMNTs, two Field Emission Electric Propulsion (FEEP) systems have been investigated for LISA and LISA Pathfinder, a caesium slit FEEP [21] and an indium needle FEEP [46], which was also con-

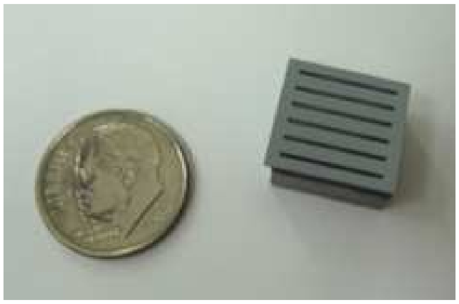

FIG. 8: SRI fabricated linear array version of the liquid metal ion source with 1 cm^2 active area. Prototypes were operated $>$ 30 hours, with multiple start/stop, and even atmospheric exposure between runs to test device robustness and physics.

sidered for the COGE mission [54]. However, no thruster has thus far demonstrated all requirements for noise, precision, dynamic range in thrust and lifetime [14]. A significant effort in micronewton propulsion technology development and testing is needed.

An attractive alternate thruster baselined for LAGRANGE is a scalable ion propulsion concept based on micro-fabricated arrays of liquid metal ion sources, currently under development at SRI International [9, 10]. Thrust is generated by the acceleration and control of independently created ions and electrons, each generated using arrays of micro-fabricated emission sites. The use of independent extraction and acceleration electrodes enables very high mass efficiency (high specific impulse) and wide dynamic range of thrust. This control approach allows smooth variation of thrust over the full operating range.

Prototype ion sources have been operated in the 1-5 W range, and ion source operation has been validated from 2,000 s to 10,000 s specific impulse. A prototype ion source is shown in Fig. 8. Because of the lower operating voltages enabled by microfabrication of ion emission sites, packaging, including control electronics and power conversion, are expected to occupy $<$ 10 cm^2. Arrays of up to 160 emitters have been tested, with prototypes able to handle up to 480 emitters; each emitter in such an array is capable of approximately 1-10 nN of thrust and can be pulsed to produce pN-sec impulse bits if each emission site is independently controlled.

The micro-fabricated scale of the elements results in rapid neutralization of the particle streams to permit high currents from such a small area device. Hence, this developing technology can be scaled to arrays of arbitrary size to provide nanonewtons to newtons of thrust while meeting all of the observatory propulsion requirements. For example, this allows these thrusters to be used for both drag-free operations and for the $\sim$ 1 m/s station keeping maneuvers needed once every 6 to 12 months.

Thermal Control System

Spacecraft heating around the outside surface varies at the orbital period of 27.3 days. The payload is kept nominally at 300 K, while the exterior sun facing solar arrays heat to roughly 350 K. The solar arrays are thermally isolated to keep exterior spacecraft components stable to 1 K, and additional thermal control on the telescopes keeps them stable to 1 mK.

The 27.3 day thermal cycle is 10^3 below the minimum science frequency of 1 mHz. This greatly reduces the thermal impact on the science instrument, which requires 10 μK $\mathrm{Hz}^{-1/2}$ temperature stability in the science band. To isolate the MGRS and optics bench from the $\sim$ 1 K spacecraft temperature variations, a nominal thermal enclosure consisting of a 2-4 alternating layers of highly conductive shields and vacuum spacing is employed. Radiative heat transfer can be further reduced by coating with low emissivity materials. Shiny gold coating reduces emissivity to $\sim$ 0.02 [37], 3.5 times less than a rough surface. A thermal control system with $<$ μK stability has been designed with COMSOL for the low earth orbiting STAR spacecraft, validating the concept[11, 35].

Drag-free and Attitude Control

Three-axis drag-free translation control keeps the spacecraft centered on the TM to within 2 nm $\mathrm{Hz}^{-1/2}$ in the measurement band. Each axis is controlled independently (no cross-coupling). The drag-free position accuracy is limited by the DOSS noise (1 nm $\mathrm{Hz}^{-1/2}$) and the dominant spacecraft disturbances, which are solar radiation pressure at 1 AU ($\lesssim 10^{-10}$ m/s^2 $\mathrm{Hz}^{-1/2}$ [47]) and micronewton thruster noise (3×10^{-10} m/s^2 $\mathrm{Hz}^{-1/2}$).

The 3-axis attitude control is completely independent from the drag-free control and aligns the two telescopes to the two remote spacecraft using wavefront sensing as in LISA. The required accuracy is 10 nm $\mathrm{Hz}^{-1/2}$ in the measurement band. The remaining degree of freedom is accommodated by telescope beam steering.

Acceleration Noise Budget

A detailed acceleration noise budget has been assembled for the MGRS. The budget contains 30 terms: 6 S/C-to-TM stiffness, 8 magnetic, 6 thermal, 4 electric, 4 Brownian, 1 cosmic ray, and 1 laser noise term. The resulting composite acceleration amplitude spectral density is shown in Fig. 9 for three possible configurations. The baseline design consists of an AuPt sphere, 70 mm in diameter with a 35 mm gap between TM and housing (green curve in Fig. 9). Also shown are the results the same geometry, but with a Berglide sphere (blue) and for an AuPt sphere with a 100 mm gap (red), demonstrating the performance scalability of the MGRS.

The TM-to-spacecraft gap size, d, is the most important design parameter with respect to acceleration noise performance. Magnetic, Electric, and the largest of the Brownian disturbances are proportional to $1/(\rho d)$ (ρ = TM density). The MGRS gap size (35 mm) and TM density (2×10^4 kg/m^2) are 1,000 and 10 times larger than that of GP-B respectively. As a cross-check, we scale the acceleration noise performance of GP-B (4×10^{-11} m/s^2 $\mathrm{Hz}^{-1/2}$

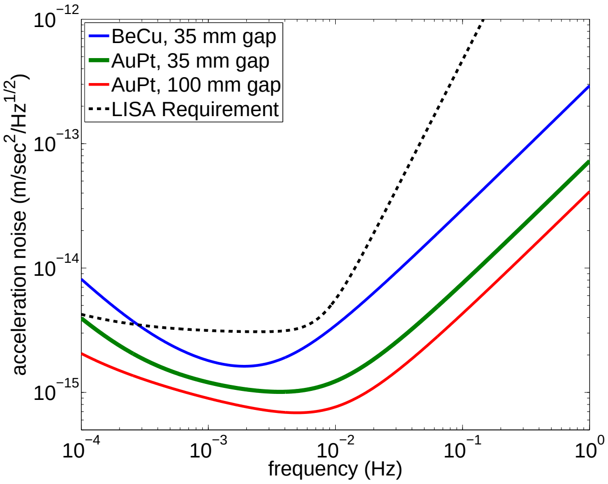

FIG. 9: Estimated MGRS acceleration noise performance for a 35 mm diameter AuPt test mass with a 35 mm gap (green), with the gap increased to 100 mm (red), and with a Berglide TM (blue). The LISA requirement is shown for comparison.

from 0.01 to 10 mHz [18]) by these ratios and obtain for the MGRS, an acceleration noise of 4×10^{-15} m/s^2 Hz$^{-1/2}$.

When constructing the acceleration noise budget shown in Fig. 9, environmental requirements below 1 mHz for spacecraft-to-TM stiffness, spacecraft temperature fluctuations, stray (patch) voltages, TM charge, and spacecraft magnetic environment were relaxed relative to LISA, some by an order of magnitude in order to simplify the spacecraft and MGRS design and reduce cost.

SPACECRAFT AND MISSION DESIGN

Spacecraft Design

The LAGRANGE spacecraft is based on an existing Lockheed configuration that has flown successfully many times. Indeed, Lockheed's vast experience, with more than 950 spacecraft flown, adds confidence to the overall LAGRANGE mission success. The spacecraft is a dodecagon structure ~3 m in diameter and ~0.7 m tall, consisting of a compact equipment section with an inner diameter center bay which accommodates the telescopes and payload. A fixed high gain antenna is mounted between the two telescopes. To minimize the telescope and payload deformations, the spacecraft material will be thermally controlled in order to maintain a low thermal gradient and a high level of thermal stability. The spacecraft equipment is mounted in the outer bays and oriented to minimize pointing error. The solar arrays consist of fixed panels mounted on the outer sides of the spacecraft structure. Radiators are located on the top and bottom of the spacecraft for thermal control.

The total mass of each LAGRANGE vehicle is < 470 kg, including payload, requiring < 500 W of power while transmitting data to the ground. The mass estimate for each component has been evaluated and assigned a maturity rating, and a contingency value assigned from Lockheed's standard weight/power growth allocation and depletion schedule based on history and experience from actual measurements of flight hardware.

TABLE III: Spacecraft and Payload mass and power budget.

	Mass* (kg)	Power** (W)
Spacecraft (× 3)		
Payload	170	175
Spacecraft	300	325
Total spacecraft + payload	470	500
Propulsion module (× 1)		
dry propulsion module	330	
propellant	230	
Launch adapter (× 1)	100	
TOTAL	**< 2,070**	

* including 30% margin for payload and propulsion module, 14% margin for > TRL 6 Lockheed spacecraft
** including 30% margin for payload, 8% margin for spacecraft, while transmitting

The spacecraft are designed for a minimum of five years of operation, easily complying with the baseline (plus IOC) LAGRANGE mission duration requirement.

Communications

Communications with the spacecraft is performed with transmitters on board each spacecraft that communicate directly with ground stations. LAGRANGE will use the standard NASA ground network, consisting of 10-11 m antennas located all over the Earth. The down-link rate is 1 Mbps and the up-link rate 1 kbps, with a 9.6 ratio of received energy per-bit to noise-density. The transmitter power is 10 watts and the half power beam width is >8 deg. An advantage of this design is that it allows near continuous communications with all three spacecraft during the initialization phase and other critical phases of the mission.

Mass and Power Budgets

Table III shows the mass and power requirements for each of the three spacecraft, as well as the total wet launch mass, including the propulsion module and launch adapter. The propulsion module carries 230 kg of bi-propellant with an Isp of 320 s. This provides a total Δv of 600 m/s to the three spacecraft stack plus an additional 30% margin.

The baseline launch vehicle is the Falcon 9 Block 2 with a 4.6 m diameter × 6.6 m tall fairing. The maximum launch mass for $C3 = 0$ kg^2/s^2 is 2,500 kg. The total wet launch mass, < 2,070 kg, which includes 30% margin, makes up only 80% of the total capacity of the Falcon 9. The mass, stack dimensions and C3 are all consistent with the more energetic Atlas V 401 and possibly smaller, less expensive launch vehicles.

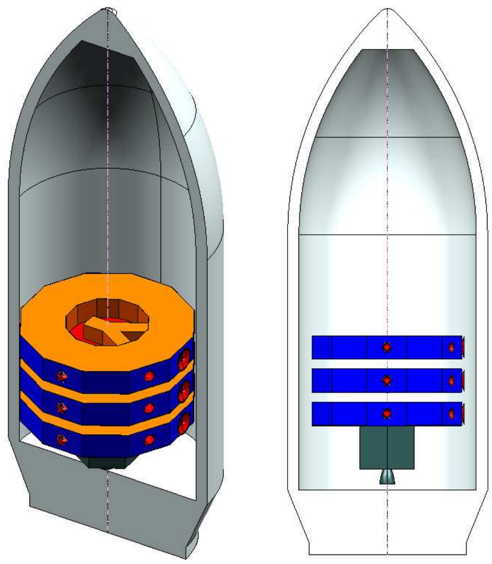

FIG. 10: Conceptual view of the three LAGRANGE spacecraft plus propulsion module inside the Falcon 9 fairing.

TABLE IV: Payload & spacecraft heritage and TRL.

Component	Heritage	TRL
Spacecraft	Lockheed	>6
Laser system	LISA Pathfinder [14]	6
Charge control	UV-LED Sat [17]	6
GRS	DISCOS [49], GP-B [29], LISA [14]	5
Laser freq. system	LISA [14], STAR	5
Phasemeter	GPS, LISA [48]	5
Caging mechanism	DISCOS [33]	5
μN thrusters	SRI [9] (CMNT[36]), In FEEP[54])	4(6)
Telescope	QuickBird [30], MTI [38]	4
PAAM	LISA [45]	4
Shadow sensor	SALKS small sat. [59]	4

Mission Design

The LAGRANGE mission is divided into four phases: (a) launch plus $\sim$ 6 month cruise to the science orbit (after which the propulsion module is ejected), (b) Initial Orbit Checkout (IOC), which includes starting drag-free operations and acquisition of the signal from the remote spacecraft, (c) 5-year science observations, and (d) decommissioning at the end of the mission.

The three spacecraft are stacked together with a single propulsion module inside the launch vehicle fairing (see Fig. 10). After separation from the launch vehicle upper stage, the propulsion module brings all three spacecraft into a phasing orbit, which lies in the plane of the moon's orbit with apogee at the lunar apogee ($\sim$ 384,000 km) and eccentricity to achieve a 33 day orbital period. This orbit is designed so that at apogee, the propulsion module and 3 spacecraft return to the moon's orbit with a 60 deg phase shift every 33 days. Every 66 days one of the three spacecraft is delivered into its Lagrange point.

Two types of low thrust injections have been identified that can achieve this phasing orbit: 1) The baseline is a direct launch to the Weak Stability Boundary (WSB), followed by a small Δv to return to the Earth-moon system, and then a lunar swing-by; 2) the alternate is a direct launch into Trans-lunar Injection (TLI) followed by a lunar swing-by coupled with a larger Δv from the propulsion module. The WSB injection lasts 9 months, requiring a C3 of 0 kg^2/s^2 and a 600 m/s total Δv from the propulsion module, while the TLI injection takes only 6-7 months and requires a C3 of -1.7 kg^2/s^2 and a 800 m/s total Δv from the propulsion module.

After reaching the science orbit, the mission lifetime is planned to be 5 years, and is only limited by the lifetime of the science instrument and micronewton thrusters. The Earth-moon L3, L4, L5 orbit can be maintained indefinitely with ~ 1 m/s Δv every 6-12 months for station keeping. During these maneuvers, the test mass must be spun-down, but not re-caged for accelerations $\sim 10^{-5}$ m/s^2.

LAGRANGE data analysis would proceed as in LISA. Phase measurements from each spacecraft are combined using TDI [15] and stored on public networks for analysis by remote science investigators. Existing LISA data analysis methodologies [16] would directly apply to the LAGRANGE data. The main difference would be the change of antenna pattern due to the different orbit.

Order-of-Magnitude Cost Estimate

LAGRANGE cost is estimated in the medium range of \$600M to \$1B. A detailed and conservative joint ARC and Lockheed Martin cost analysis puts the mission ROM cost at \$950M FY12, including 30% reserves. LM has orbited over 950 S/C, supporting many relevant programs that have segments, subsystems or components similar to LAGRANGE and were used to get actual cost data. The non-recurring costs for the development of 3 identical spacecraft whose hardware elements are all TRL 6 or greater has been accounted for. The payload ROM cost was developed using a combination of bottoms-up and analogies based on major components. ROM cost for the remaining mission elements used a WRAP factor applied on the hardware costs (spacecraft and payload), modeled on similar size and complexity missions and derived from the NASA ARC cost database of these missions. Simplistically using the function describing the historical mission cost data we obtain estimates in the \$640M to \$895M FY 11, depending on assumptions about the cost of 3 identical systems.

TECHNOLOGY READINESS

Table IV shows the flight heritage and TRL for each of the main LAGRANGE sub-systems. Except for a few sub-components, all sub-systems are at TRL 5 or higher.

Appendix A: Acknowledgments

Leo Hollberg (Stanford) for his knowledge and experience with optical cavities and laser interferometers, Ke-Xun Sun (University of Nevada, Las Vegas) for several technical contributions, Stefano Vitale (University of Trento) for insights into the LISA and LISA Pathfinder GRS, Ron Hellings (Montana State University) for engineering and science implications of geocentric gravity-wave observatories and telescope filters, Cesar Ocampo (University of Texas, Austin) for initial information regarding Earth-moon Lagrange points, Vlad Hruby (Busek) for input on FEEPs and their spacecraft integration, and the entire LISA team for their contributions to this field over the past few decades.

Appendix B: References

[1] email address and contact informaiton for John W. Conklin, primary submitter, research associate, johnwc@stanford.edu, 1-650-721-2065.

[2] email addresses for CrossTrac team: hanson@netwizards.net.

[3] email addresses for KACST team: aljadaan@stanford.edu; alfauwaz@stanford.edu malmajed@kacst.edu.sa; haltwaijry@kacst.edu.sa; talsaud@kacst.edu.sa.

[4] email addresses for Lockheed Martin team: daniel.r.bower@lmco.com; bill.costello@lmco.com; ken.hooper@lmco.com; aklavins@msn.com; alice.palmer@lmco.com; barbara@borealinfotech.com; david.schaechter@lmco.com; tom.sherrill@lmco.com; eric.h.smith@lmco.com; ker-li.shu@lmco.com; domenick.tenerelli@lmco.com; roel.vanbezooijen@lmco.com; gopal.vasudevan@lmco.com.

[5] email addresses for NASA ARC team: dohy.m.faied@nasa.gov; cyrus.foster@nasa.gov; anthony.genova@nasa.gov; jaroux@nasa.gov; hugo.sanchez@nasa.gov; pete.worden@nasa.gov.

[6] email addresses for SRI team: scott.williams@sri.com; victor.aguero@sri.com.

[7] email addresses for Stanford team: sbuchman@stanford.edu; karthikb@stanford.edu; rlbyer@stanford.edu; cutlerg@stanford.edu; ddebra@stanford.edu; hultgren@stanford.edu; blantz@stanford.edu; jlipa@stanford.edu; saraf@stanford.edu; zoellner@stanford.edu.

[8] Falcon 9 Launch Vehicle Payload User's Guide, Rev. 1. 2009.

[9] V. M. Aguero. Experimental Results and Considerations on Use of Field Emission Devices in Space. AIAA Joint Propulsion Conference Proceedings, AIAA 2001-3338, July 2001.

[10] V. M. Aguero. High Efficiency Ion Thruster. SRI final report for DARPA/TTO, Contract MDA972-02-C-0073, 2003.

[11] A. Alfauwaz and K.-X. Sun. Design and Modeling of Highly Stable and Uniform Thermal Enclosure for Precision Space Experiment. In *Journal of Physics Conference Series*, Proceedings of the 8th International LISA Symposium, 2011.

[12] G. Allen, J. W. Conklin, K-X. Sun, D. B. DeBra, and R. L. Byer. Mass Center Position Determination of a Spinning Sphere as part of a Modular Gravitational Reference Sensor. to be submitted; preprint available at: https://spacegrav.stanford.edu/MGRS.

[13] G. S. Allen. *Optical Sensor Design for Advanced Drag-free Satellites*. PhD thesis, Stanford University, 2009.

[14] F. Antonucci et al. LISA Pathfinder: mission and status. *Classical and Quantum Gravity*, 28(9):094001–+, May 2011.

[15] J. W. Armstrong, F. B. Estabrook, and M. Tinto. Time-Delay Interferometry for Space-based Gravitational Wave Searches. *Astrophys. J.* , 527:814–826, December 1999.

[16] S. Babak, J. G. Baker, M. J. Benacquista, N. J. Cornish, J. Crowder, S. L. Larson, E. Plagnol, E. K. Porter, M. Vallisneri, A. Vecchio, T. M. L. Data Challenge Task Force, K. Arnaud, L. Barack, A. Błaut, C. Cutler, S. Fairhurst, J. Gair, X. Gong, I. Harry, D. Khurana, A. Królak, I. Mandel, R. Prix, B. S. Sathyaprakash, P. Savov, Y. Shang, M. Trias, J. Veitch, Y. Wang, L. Wen, J. T. Whelan, and t. Challenge-1B participants. The Mock LISA Data Challenges: from Challenge 1B to Challenge 3. *Classical and Quantum Gravity*, 25(18):184026, September 2008.

[17] K. Balakrishnan, E. Hultgren, J. Goebel, and K.-X. Sun. Space Qualification Test Results of Deep UV LEDs for AC Charge Management. In *11th Spacecraft Charging Technology Conference*, poster presentation, September 2011.

[18] W. J. Bencze, D. B. DeBra, L. Herman, T. Holmes, G. M. Keiser, and C. W. F. Everitt. On-orbit performance of the Gravity Probe B drag-free translation control system. In *Proceedings of the 29th AAS Cuidance and Conrol Conference*, 2006.

[19] P. Bender et al. LISA, Laser Interferometer Space Antenna for the detection and observation of gravitational waves. LISA Pre Phase A Report, 233, Max-Plank-Institut für Quantenoptik, Garching, Germany, July 1998.

[20] S. Buchman, R. L. Byer, J. Hanson, D. B. DeBra, D. L. Klinger, S. D. Williams, L. D. Dewell, D. B. Schaechter, N Pedreiro, and D. J. Tenerelli. Gravitational Reference Technologies: Critical for U.S. Space Leadership, a white paper. 2004.

[21] F. Ceccanti, L. Paita, U. Cesari, M. DeTata, N. Giusti, P. Balducci, and M. DelPistoia. 3200 hours Endurance Testing of the LISA Pathfinder FT-150 Thruster. In *Proceedings of the 31st International Electric Propulsion Conference*, AIAA-06-4826, 2009.

[22] J. W. Conklin. *Estimation of the Mass Center and Dynamics of a spherical test mass for Gravitational Reference Sensors*. PhD thesis, Stanford University, 2009.

[23] J. W. Conklin, G. Allen, K-X. Sun, and D. B. DeBra. Determination of Spherical Test Mass Kinematics with A Modular Gravitational Reference Sensor. *Journal of Guidance, Control, and Navigation*, 31(6):1700–1707, November 2008.

[24] J.W. Conklin, K.-X. Sun, and D.B. DeBra. Sphere mass center determination by velocity modulation. *Precision Engineering*, 35(3):464 – 472, 2011.

[25] D. B. Debra. Design considerations for drag free satellites. In W. M. Folkner, editor, *Laser Interferometer Space Antenna, Second International LISA Symposium on the Detection and Observation of Gravitational Waves in Space*,

volume 456 of *American Institute of Physics Conference Series*, pages 199–206, December 1998.

[26] D. B. DeBra and J. W. Conklin. Measurement of drag and its cancellation. *Classical and Quantum Gravity*, 28(9):094015, May 2011.

[27] R. Dolesi, D. Bortoluzzi, P. Bosetti, L. Carbone, A. Cavalleri, I. Cristofolini, M. Da Lio, G. Fontana, V. Fontanari, B. Foulon, C. D. Hoyle, M. Hueller, F. Nappo, P. Sarra, D. N. A. Shaul, T. Sumner, W. J. Weber, and S. Vitale. Gravitational sensor for LISA and its technology demonstration mission. *Classical and Quantum Gravity*, 20:99, May 2003.

[28] R. W. P. Drever, J. L. Hall, F. V. Kowalski, J. Hough, G. M. Ford, A. J. Munley, and H. Ward. Laser phase and frequency stabilization using an optical resonator. *Applied Physics B: Lasers and Optics*, 31:97–105, 1983. 10.1007/BF00702605.

[29] C. W. F. Everitt, D. B. Debra, B. W. Parkinson, J. P. Turneaure, J. W. Conklin, M. I. Heifetz, G. M. Keiser, A. S. Silbergleit, T. Holmes, J. Kolodziejczak, M. Al-Meshari, J. C. Mester, B. Muhlfelder, V. G. Solomonik, K. Stahl, P. W. Worden, Jr., W. Bencze, S. Buchman, B. Clarke, A. Al-Jadaan, H. Al-Jibreen, J. Li, J. A. Lipa, J. M. Lockhart, B. Al-Suwaidan, M. Taber, and S. Wang. Gravity Probe B: Final Results of a Space Experiment to Test General Relativity. *Physical Review Letters*, 106(22):221101, June 2011.

[30] J. W. Figoski. Alignment and test results of the QuickBird telescope using the Ball Optical System Test Facility. In W. Roybal, editor, *Society of Photo-Optical Instrumentation Engineers (SPIE) Conference Series*, volume 3785 of *Society of Photo-Optical Instrumentation Engineers (SPIE) Conference Series*, pages 99–108, October 1999.

[31] Committee for a Decadal Survey of Astronomy and Astrophysics; National Research Council. *New Worlds, New Horizons in Astronomy and Astrophysics*. The National Academies Press, Washington, D.C., 2010.

[32] D. Gerardi, G. Allen, J. W. Conklin, K. Sun, D. DeBra, S. Buchman, P. Gath, W. Fichter, R. L. Byer, and U. Johann. Advanced drag-free concepts for future space-based interferometers: acceleration noise performance. *ArXiv e-prints*, October 2009.

[33] R. Hacker, J. Mathiesen, and D. B. DeBra. Caging Mechanism for a Drag-Free Satellite Position Sensor. In *Proceedings of the JPL 10th Aerospace Mechanism Symposium*, page 125, April 1976.

[34] A. Harper, M. Ryschkewitsch, A. Obenschain, and R Day. General Environmental Verification Standard (GEVS) for GSFC Flight Programs and Projects. April 2005.

[35] S. Higuchi, K.-X. Sun, D. B. DeBra, S. Buchman, and R. L. Byer. Design of a highly stable and uniform thermal test facility for MGRS development. *Journal of Physics Conference Series*, 154(1):012037, March 2009.

[36] V. Hruby, D. Spence, N. Demmons, T. Roy, E. Ehrbar, J. Zwahlen, R. Martin, J. Ziemer, T. M. Randolph, W. Connolly, S. Rhodes, and W. Tolman. ST7-DRS Colloid Thruster System Development and Performance Summary. In *Proceedings of the 44th AIAA/ASME/SAE/ASEE Joint Propulsion Conference and Exhibit*, AIAA2008-4826, 2008.

[37] M. Jin and S. Liang. An Improved Land Surface Emissivity Parameter for Land Surface Models Using Global Remote Sensing Observations. *Journal of Climate*, 19:2867, 2006.

[38] R. R. Kay, S. C. Bender, T. D. Henson, D. A. Byrd, J. L. Rienstra, M. L. Decker, N. G. Rackley, R. L. Akau, J. P. Claassen, R. E. Kidner, R. B. Taplin, D. M. Bullington, K. D. Marbach, C. E. Lanes, C. K. Little, B. W. Smith, B. C. Brock, and P. G. Weber. Multispectral Thermal Imager (MTI) payload overview. In M. R. Descour & S. S. Shen, editor, *Society of Photo-Optical Instrumentation Engineers (SPIE) Conference Series*, volume 3753 of *Society of Photo-Optical Instrumentation Engineers (SPIE) Conference Series*, pages 347–358, October 1999.

[39] G. M. Keiser. Gravity Probe B. In *Proceedings of the International School of Physics "Enrico Fermi", Atom Optics and Space Physics*, IOS Press.

[40] G. M. Keiser, S. Buchman, D. B. DeBra, and E. Gustafson. Advantages and Disadvantages of a Spherical Proof Mass for LISA. Presented at COSPAR 2000.

[41] Y. Kremer, J.-F. Léger, R. Lapole, N. Honnorat, Y. Candela, S. Dieudonné, and L. Bourdieu. A spatio-temporally compensated acousto-optic scanner for two-photon microscopy providing large field of view. *Optics Express*, 161:10066, June 2008.

[42] R. N. Lang and S. A. Hughes. Advanced localization of massive black hole coalescences with LISA. *Classical and Quantum Gravity*, 26(9):094035, May 2009.

[43] B. Lange. *The Control and use of Drag-free Satellites*. PhD thesis, Stanford University, 1964.

[44] J. C. Livas, J. I. Thorpe, K. Numata, S. Mitryk, G. Mueller, and V. Wand. Frequency-tunable pre-stabilized lasers for LISA via sideband locking. *Classical and Quantum Gravity*, 26(9):094016, May 2009.

[45] J. Pijnenburg, N. Rijnveld, and B. Sheard. Picometer stable scan mechanism for gravitational wave detection in space: LISA PAAM. In *38th COSPAR Scientific Assembly*, volume 38, pages 3758–+, 2010.

[46] C. Scharlemann, N. Buldrini, R. Killinger, M. Jentsch, A. Polli, L. Ceruti, L. Serafini, D. DiCara, and D. Nicolini. Qualifciation test series of the indium needle feep micropropulsion system for lisa pathfinder. *Acta Astronautica*, 69(9-10):822 – 832, 2011.

[47] Bonny L. Schumaker. Disturbance reduction requirements for LISA . *Classical and Quantum Gravity*, 20:S239–S253, April 2003.

[48] D. Shaddock, B. Ware, P. G. Halverson, R. E. Spero, and B. Klipstein. Overview of the LISA Phasemeter. In S. M. Merkovitz & J. C. Livas, editor, *Laser Interferometer Space Antenna: 6th International LISA Symposium*, volume 873 of *American Institute of Physics Conference Series*, pages 654–660, November 2006.

[49] Staff Of The Space Department, Staff Of The Guidance, and Control Laboratory. A Satellite Freed of all but Gravitational Forces: "TRIAD I". *Journal of Spacecraft and Rockets*, 11:637–+, September 1974.

[50] K.-X. Sun, A. Alfauwaz, M. Alrufaydah, H. Altwaijry, K. Balakrishnan, S. Buchman, R. L. Byer, J. W. Conklin, D. B. DeBra, J. Goebel, E. Hultgren, and A. Zoellner. Modular Gravitational Reference Sensor (MGRS) Technology Development. In *Proceedings of the 8th International LISA Symposium*, Journal of Physics Conference Series, 2011.

[51] K.-X. Sun, B. A. Allard, R. L. Byer, and S. Buchman. Charge management of electrically isolated objects via modulated photoelectric charge transfer, US patent US20080043397.

[52] K.-X. Sun, G. Allen, S. Buchman, R. L. Byer, J. W. Conklin, D. B. DeBra, D. Gill, A. Goh, S. Higuchi, P. Lu, N. A. Robertson, and A. J. Swank. Progress in Developing the

Modular Gravitational Reference Sensor. In *Laser Interferometer Space Antenna: 6th International LISA Symposium*, volume 873 of *American Institute of Physics Conference Series*, pages 515–521, November 2006.

[53] K.-X. Sun, N. Leindecker, S. Higuchi, J. Goebel, S. Buchman, and R. L. Byer. UV LED operation lifetime and radiation hardness qualification for space flights. *Journal of Physics Conference Series*, 154(1):012028–+, March 2009.

[54] M. Tajmar, A. Genovese, and W. Steiger. Indium field emission electric propulsion microthruster experimental characterization. *Journal of propulsion and power*, 20(2):211–218, 2004.

[55] M. T. Valentine, N. R. Guydosh, B. Gutiérrez-Medina, A. N. Fehr, J. O. Andreasson, and S. M. Block. Precision steering of an optical trap by electro-optic deflection. *Optics Letters*, 33:599, March 2008.

[56] C. L. Wainwright and T. A. Moore. Observing the positions of spinning binary systems using LISA. *Phys. Rev. D* , 79(2):024022, January 2009.

[57] S. P. Worden, T. Al-Saud, M. Almajed, H. Altwaijry, C. Braxmaier, S. Buchman, R. Byer, M. Cruise, M. Daniels, D. DeBra, H. Dittus, J. Goebel, J. Hall, B. Jaroux, C. Laemmerzahl, J. Lipa, A. Peters, and K.-X. Sun. Technology Development for Fundamental Physics on Small Satellites. Micrograv 2010 White Paper for Fundamental Physical Science, 2010.

[58] J. Ziemer, T. M. Randolph, G. W. Franklin, V. Hruby, D. Spence, N. Demmons, T. Roy, E. Ehrbar, J. Zwahlen, R. Martin, and W. Connolly. Delivery of colloid micronewton thrusters for the space technology 7 mission. In *Proceedings of the 44th AIAA/ASME/SAE/ASEE Joint Propulsion Conference and Exhibit*, AIAA2008-4826, 2008.

[59] A. Zoellner, E. Hultgren, M. Trittler, K.-X. Sun, and R. L. Byer. Integrated Differential Object Shadow Sensor (DOSS) for Modular Gravitational Reference Sensor (MGRS). In *Proceedings of the 8th International LISA Symposium*, Journal of Physics Conference Series, 2011.